IOP Conf. Series: Materials Science and Engineering **381** (2018) 012104 doi:10.1088/1757-899X/381/1/012104

Preparation and Dielectric Characterization of Ce-Doped $BaTiO_3$ Nanotubes

Yang Liu[a], Xiangyun Deng[b,*], Juntai Chen[c] and Qiqi Zhou[d]

College of Physics and Materials Science, Tianjin Normal University, Tianjin 300387, China
Email: [a]1412311964@qq.com, [b]xiangyundtj@126.com, [c]1332430067@qq.com, [d]294766425@qq.com

Abstract. In this paper, the microstructure and dielectric properties of $Ba_{1-x}Ce_{2x/3}TiO_3$ nanotubes were studied by hydrothermal method. TiO_2 nanotubes were prepared by anodic oxidation method and $Ba_{1-x}Ce_{2x/3}TiO_3$ nanotubes were prepared by hydrothermal synthesis using TiO_2 nanotubes as template. The films were characterized by scanning electron microscopy, X-ray diffraction .The microstructure and dielectric properties of $Ba_{1-x}Ce_{2x/3}TiO_3$ nanotubes at different $(CH_3CO_2)_3Ce \cdot xH_2O$ concentration and annealing temperature were investigated. The experimental results show that increasing the concentration of $(CH_3CO_2)_3Ce \cdot xH_2O$ and adjusting the temperature of anneal are beneficial to the transition of TiO_2 nanotubes to $Ba_{1-x}Ce_{2x/3}TiO_3$ nanotubes and improve the crystallinity, and the results are shows that in the $(CH_3CO_2)_3Ce \cdot xH_2O$ doping concentration of 0.02mol/L, annealing temperature of 300 ℃ the surface morphology of $Ba_{1-x}Ce_{2x/3}TiO_3$ nanotubes is the best. The samples have permittivity 809 and dielectric loss 0.02-0.04 under the conditions of 500 ℃ annealing temperature and 0.02 mol/L $(CH_3CO_2)_3Ce \cdot xH_2O$ concentration.

1. Introduction

Cerium is the second element in the lanthanide series with atomic number 58. Cerium is always being found in monazite and bastn äsite, it is the most common of the lanthanides. While it often shows the +3 oxidation state characteristic, it also exceptionally has a stable +4 state. Generally speaking, the Ce^{3+} occupies the Ba^{2+}site and the Ce^{4+} occupies the Ti^{4+}site.This effect is caused by the different ionic radius between the $Ce^{3+}$and Ce^{4+}[1,3].But when the doping ratio of Ce^{3+} is over 0.2 atm%, the Ce^{3+} will be incorporated into the Ti^{4+} site [4,7].

A little research has been done on the subject of the Ce-Doped $BaTiO_3$ film .The previous study indicated that in the Ce-Doped $BaTiO_3$ ceramics which were fabricated using solid state sintered technology, with the increasing of dopant content, the grains grew up, the lattice parameters were reduced and the activation energy increased [8,10]. Moreover, with the increase of the working frequency, the dielectric constants of the sample decreased. Literature about in situ diffusive phase transition behaviors of Ce^{3+}/Ce^{4+} -Doped $BaTiO_3$ film at the Curie point has been reported. The film has high dielectric constant and low dielectric loss. $Ba_{0.95}Ce_{0.05}Ti_{0.9875}O_3$ nanowires were fabricated by sol–gel method using a polycarbonate membrane with channels of 100nm diameter as template. FE-SEM analyses showed that continuous gel wires of length up to 17μm and an average diameter of 81nm were obtained [11, 16]. After calcination at 700 ℃ for 1h, these green 1D nanostructures were converted into well-crystallized wires with an average diameter of 59.7nm. The results of PFM measurements indicated that the wires exhibit a significant fraction of ferroelectric domains larger than the grains size and a good piezoelectric response.

The study on Ce doped $BaTiO_3$ film is of great significance, the electrical performance of Ce doped $BaTiO_3$ film can improve due to the combined special nanotube structure and doping methods.

2. Experimental

2.1. Process of preparing sample

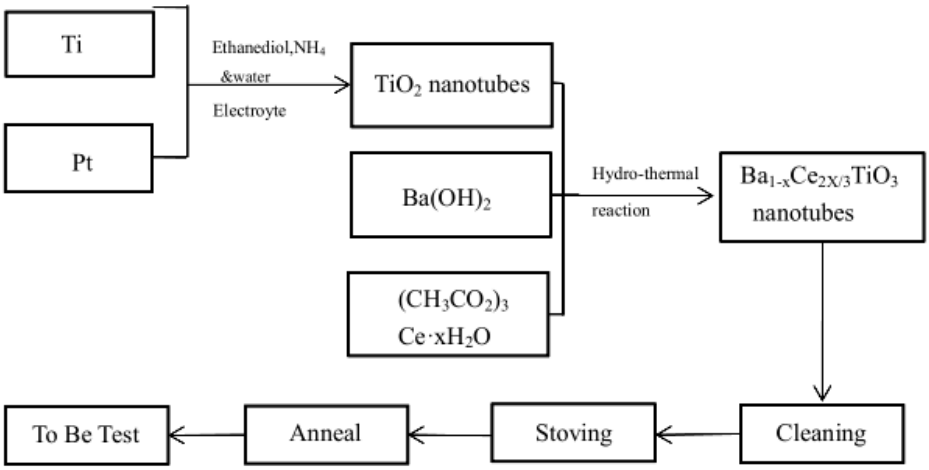

Figure 1. $Ba_{1-x}Ce_{2X/3}TiO_3$ nanotubes preparation process.

The process of preparing $Ba_{1-x}Ce_{2X/3}TiO_3$ nanotubes is shown in Figure 1. Firstly clean the titanium plate respectively in C_3H_6O, CH_3OH, C_3H_8O and ultrasonic after grinding, after drying, as anode, foil as the cathode to anodic oxidation reaction. In this paper, TiO_2 nanotubes arrays are prepared in the electrolyte was 0.25 wt % NH_4F +150mL of $HOCH_2$-CH_2OH + 5mL distilled water with electrode distance 2cm, oxidation voltage 50V, oxidation time 4h [17,18]. Then put the TiO_2 nanotubes in Ba $(OH)_2$ and $(CH_3CO_2)_3Ce \cdot xH_2O$ solution and the reaction in the muffle furnace,$Ba_{1-x}Ce_{2X/3}TiO_3$ nanotubes are prepared by the hydrothermal synthesis method, control the concentration of $(CH_3CO_2)_3Ce \cdot xH_2O$ and annealing temperature separately. The $Ba(OH)_2$ and $(CH_3CO_2)_3Ce \cdot xH_2O$ solution for different quality of $Ba(OH)_2$ and$(CH_3CO_2)_3Ce \cdot xH_2O$ + 75mL distilled water, TiO_2 nanotubes are vertical in the water to ensure the TiO_2 nanotubes in dictating responding well and the solution, then tighten the water hot kettle, guarantee not leak, into the reaction in the muffle furnace. Set the heating speed of 2 ℃ /min from room temperature up to 200 ℃ and heat preservation time of 6h, and finally down to room temperature.

2.2. Test

The $Ba_{1-x}Ce_{2x/3}TiO_3$ nano-tubes were characterized by Xray diffraction (D/MAX-2500). Morphology features of the $Ba_{1-x}Ce_{2x/3}TiO_3$ nano-tubes were investigated using TEM (S4800/TM3000).The electrical properties of the nanotubes were investigated and analyzed.

Table 1. Preparation parameters of $Ba_{1-x}Ce_{2x/3}TiO_3$nano-tubes

Number	$(CH_3CO_2)_3Ce \cdot xH_2O$ concentration/(mol/L)	Hydrothermal Temperature (℃)	annealing time (h)	annealing temperature (℃)
1	0	200 °	2	300 °
2	0.002	200 °	2	300 °
3	0.005	200 °	2	300 °
4	0.008	200 °	2	300 °
5	0.002	200 °	2	300 °
6	0.002	200 °	2	400 °
7	0.002	200 °	2	500 °

3. Crystal structure analysis

3.1. Different concentration of $(CH_3CO_2)_3Ce{\cdot}xH_2O$

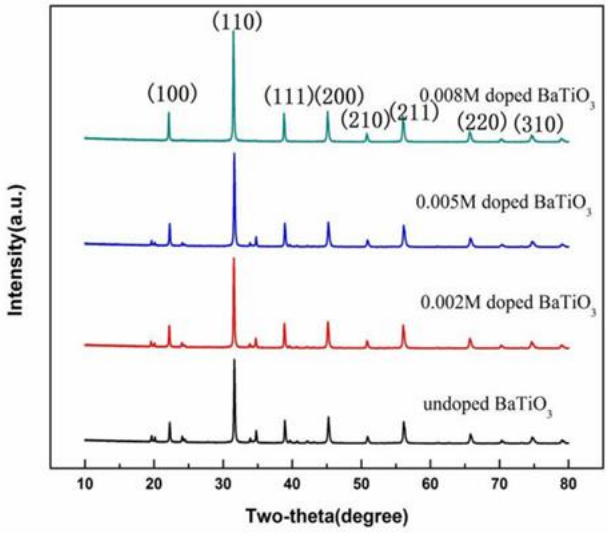

Figure 2. XRD patterns of $Ba_{1-x}Ce_{2x/3}TiO_3$ nanotubes prepared with different $(CH_3CO_2)_3Ce{\cdot}xH_2O$ concentration.

The spectrogram shows that 4 samples all have (100), (110), (111), (200), (210) and (211) crystal face diffraction peak. The X-ray diffraction lines can be indexed to a cubic phase of $BaTiO_3$. Element Ce along with it's oxide can't be observed in Figure 2 indicating that Ce ions have entered the unit cell. This is because the Ce^{3+} occupies the Ba^{2+}site and the Ce^{4+} occupies the Ti^{4+}site [19].Meanwhile the XRD data indicate that the Ce doping causes the XRD peaks to broaden. According to $D=K\lambda/(\beta\cos\theta)$, the size of grain can be getted. The results are shown in Table 2.

Table 2. Lattice parameters and grain size of BCT2 nanotubes at different $(CH_3CO_2)_3Ce{\cdot}xH_2O$ concentration.

$(CH_3CO_2)_3Ce{\cdot}xH_2O$ concentration/(mol/L)	structure	a(Å)	c(Å)	c/a	Grain size(nm)
0	cubic	4.0071	4.0071	1	75.8
0.002	cubic	4.00958	4.00958	1	69.9
0.005	cubic	4.01445	4.01445	1	64.6
0.008	cubic	4.01648	4.01648	1	60.2

When the Ce concentration increasing, the grain sizes become smaller and the degrees of crystallization increase. The reason is that Ce ions are adsorbed on the surface of the grain, defects appeared, the growth of grain is suppressed. It's also due to the smaller ionic radius of the Ce^{3+} (0.118 nm)compared with that of the Ba^{2+}(0.135 nm). Table 2 shows that with increasing dopant content, the lattice constant a becomes larger. We infer that with more Ce enters the unit cell of $BaTiO_3$, the degree of lattice distortion increase.

Table 3. Lattice parameters and grain size of BCT2 nanotubes at different annealing temperature.

Annealing temperature	structure	a(Å)	c(Å)	c/a	Grain size(nm)
300 ℃	tetragonal	3.9898	4.0035	1.00343	75.6
400 ℃	tetragonal	4.0018	4.0064	1.00115	73.9
500 ℃	tetragonal	4.0017	4.0050	1.00083	74.5

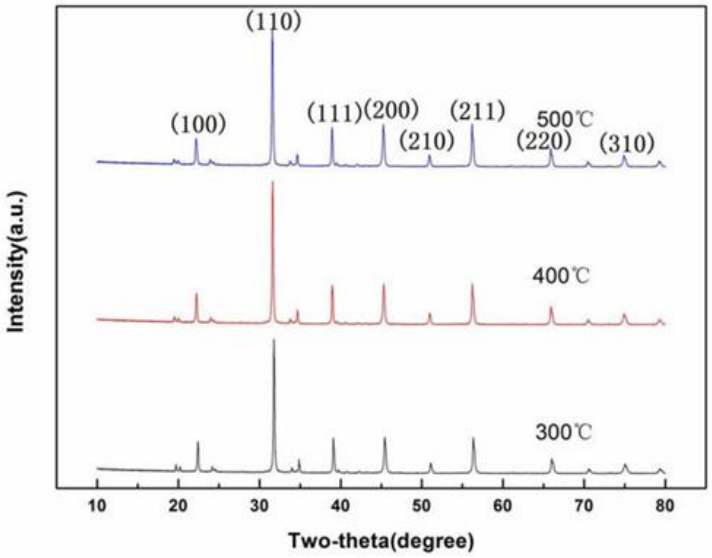

Figure 3. XRD pattern of BCT2 nanotubes at different annealing temperature.

From figure 3, we can conclude that after annealing, the composition of the sample is tetragonal phase of $BaTiO_3$.From table 3; we can see that when the annealing temperature is 300 ℃, the grain sizes become larger. This phenomena is caused by annealing recrystallization. The fault caused by Ce adsorbed on the surface of the grain is healed partially, the grain can grow normally. When the annealing temperature is 400 ℃, the grain sizes become smaller. We guess that with more defects were healed; Ce adsorbed on the surface reenters the unit cell of $BaTiO_3$. Ionic radius difference between Ba^{2+} and Ce^{3+} lead to the grain sizes become larger, the degree of lattice distortion increase and the lattice constant a becomes larger. When the annealing temperature is 500 ℃, the defects disappear, the grain can grow again.

3.2. Surface morphology

3.2.1. Different concentration of $(CH_3CO_2)_3Ce\ xH_2O$ /(mol/L)

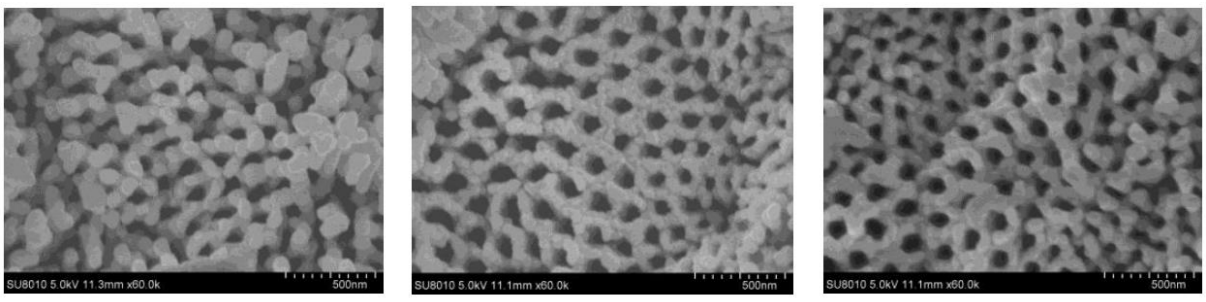

0.002 mol/L 0.005 mol/L 0.008 mol/L

Scanning electron micrographs (SEM) of the resulting samples prepared at different concentrations of cerium acetate are shown. It can be seen in the figure that the formed $Ba_{1-x}ce_{2x/3}TiO_3$ nanotubes are still tubular structures, and the wall of the tube is thickened with some protrusions on the surface. This is due to the volumetric effect of TiO_2 nanotubes transformed into $Ba_{1-x}ce_{2x/3}TiO_3$ nanotubes. With the increase of Ce doping, the grain size of nanotubes becomes smaller. As the grains become smaller, resulting in gaps between the tube and the tube, the pore size becomes about 80 ~ 95 nm, larger than pure barium titanate.

3.2.2. Different annealing temperature

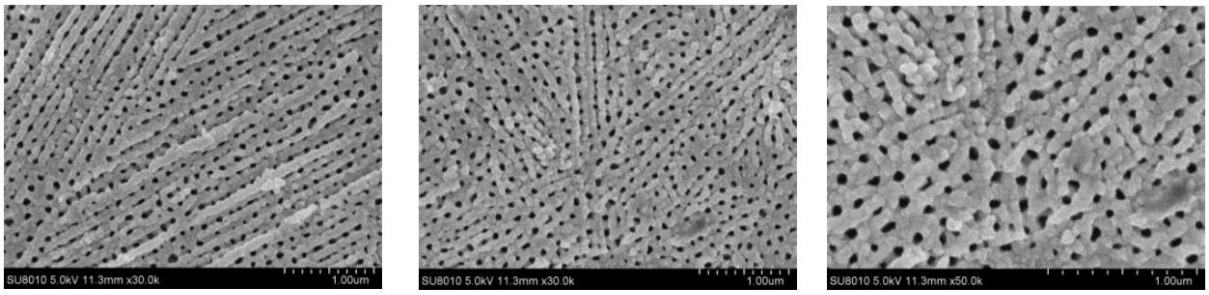

300° 400° 500°

Careful observation from the figure can be drawn, the $Ba_{1-x}ce_{2x/3}TiO_3$ nanotubes prepared at different annealing temperatures remain nanotubular structure, with the annealing temperature increases, the wall thickens, the inner diameter decreases, some grains grow into nanoparticles covering the surface of the tube.

3.3. Dielectric properties

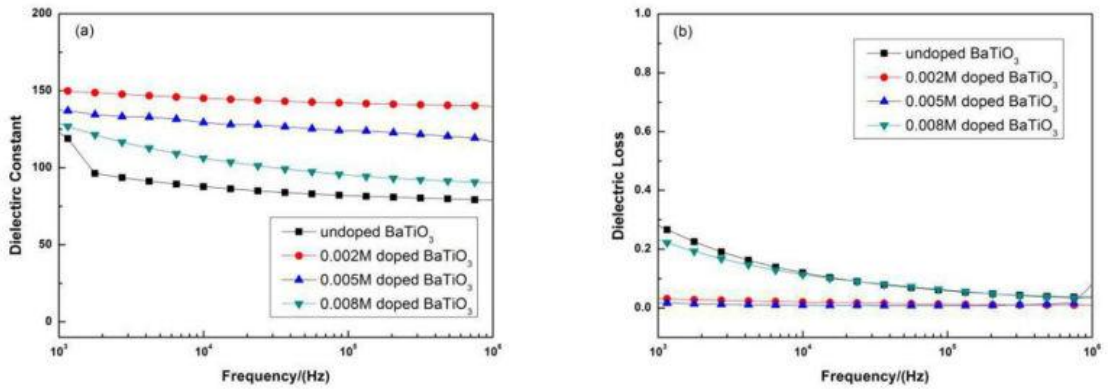

Figure 4. Dielelctric constant (a) and dielelctric loss (b) depend on frequency for BCT0/2/5/8 nanotubes at room temperature.

Figure 4 shows the relationship between the dielectric constant (a) and the dielectric loss (b) of $Ba_{1-x}Ce_{2x/3}TiO_3$ nanotubes at room temperature under different ce concentrations. First of all, the height of several curves in Figure 3.6 (a) shows that the dielectric constant of samples increases first and then decreases with the increase of Ce content, which is the highest at BCT2. This may be due to the doping of Ce , So that the crystal grain size of BCT nanotubes becomes smaller, surface effect occurs on the surface of the nanoparticle, the surface tension of the particles becomes larger, so that the crystal lattice distortion, the lattice constant a becomes larger, self-polarization ability increases, resulting in improved dielectric properties. The subsequent decrease in dielectric constant is due to the fact that more and more Ce^{3+} replaced Ba^{2+} resulted in the shrinkage of oxygen octahedra, the decrease of oxygen vacancies, the decrease of grain growth and the decrease of relative displacement of Ti^{4+} Self-polarization is also reduced, resulting in a decrease in dielectric constant. It can be seen from Figure (B) that the Ce doping is in the range of 103Hz ~ 106Hz, the dielectric loss is between 0.01 ~ 0.3, especially BCT2 / 5, the dielectric loss is as low as 0.02-0.04. As can be seen from the figure, proper addition of Ce can improve the dielectric properties of barium titanate nanotube.

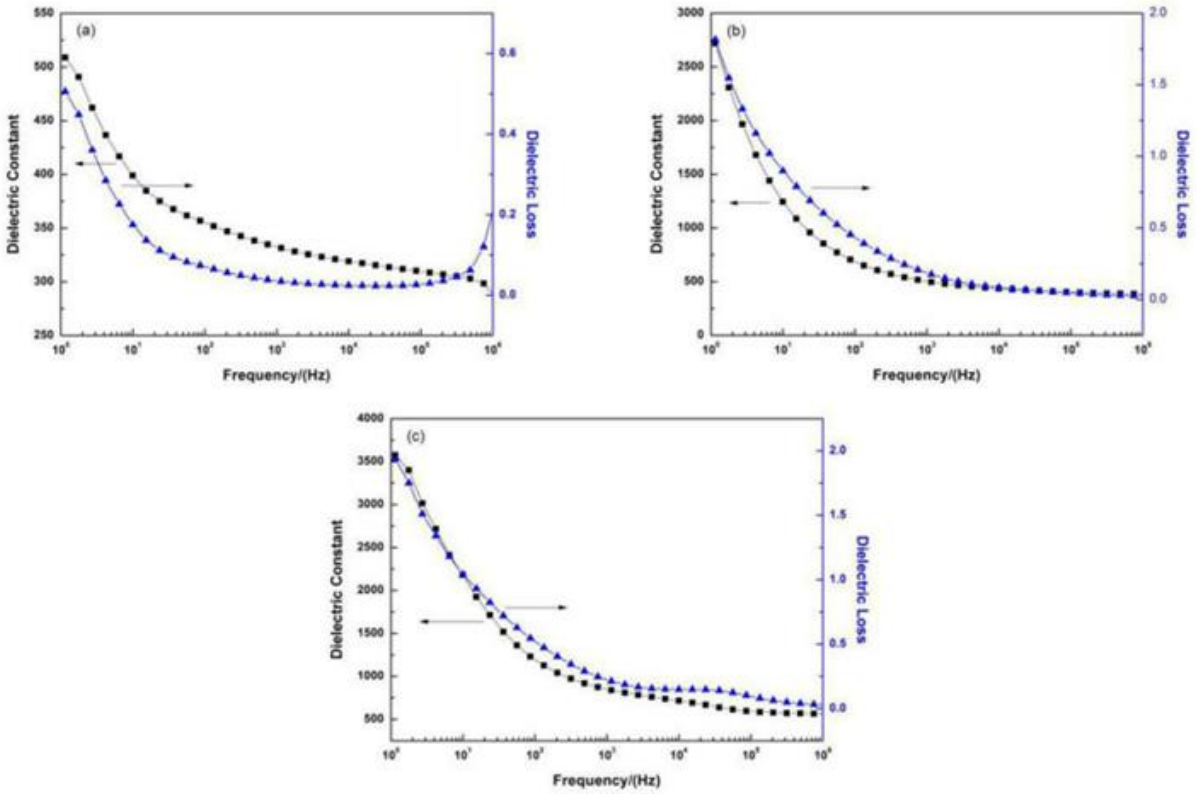

Figure 5. Dielectric constant and dielectric loss depend on frequency of BCT2 nanotubes at different annealing temperature.

Figure 5 shows the dielectric constant and dielectric loss versus frequency for $(CH_3CO_2)_3Ce \cdot xH_2O$ 0.02mol / L $Ba_{1-x}Ce_{2x/3}TiO_3$ nanotubes at different annealing temperatures. Figure (a) is annealed at 300 °C; Figure (b) is annealed at 400 ℃; and Figure (c) is annealed at 500 ℃. It can be clearly seen from the figure that the dielectric constant becomes larger after annealing because the phase transition from cubic phase to tetragonal phase after annealing is greatly enhanced and the dielectric constant is increased. With the increase of annealing temperature, the dielectric properties further improve, respectively 331, 495 and 809, with the pure titanium titanate annealing point of view, a great increase. Dielectric loss in the frequency range of 103Hz ~ 106Hz, at 0.1 or so, but a little higher than before, but the rise is extremely limited.

4. Acknowledgements

This project was funded by Tianjin Normal University (Grant No. 53H14049).

5. References

[1] Agantsev A, Sherman V, Astafiev K, et al. Ferroelectric materials for microwave tunable applications [J]. J. Electrocera., 2003, 11(1): 5 - 66.
[2] Araujo A P D, Cuchiaro J D, McMillan L D, et al. Fatigue-free ferroelectric capacitors with platinum electrodes [J]. Nature International Weekly Journal of Science, 1995, 374 (6523): 627-629.
[3] Bokov A A, Ye Z G. Phenomenological description of dielectric permittivity peak in relaxor ferroelectrics [J]. Solid State Communications, 2000, 116(2):105-108.
[4] Busch G. Investigations on Influence of Engine Block Design Features on Noise and Vibration [J]. Condensed Matter News, 1991, 1(2): 20.
[5] Chen D, Zhang H T, Chen R K, et al. Well-ordered arrays of ferroelectric single-crystalline BaTiO3 nanostructures [J]. Physica Status Solidi, 2012, 209 (4):714- 717.

[6] Chen H, Yang C, Fu C, et al. The size effect of Ba0.6Sr0.4TiO3, thin films on the ferroelectric properties [J]. Applied Surface Science, 2006, 252 (12): 4171- 4177.
[7] Chen Y Y, Yu B Y, Wang J H, et al. Template-based fabrication of SrTiO3 and BaTiO3 nanotubes. [J]. Inorganic Chemistry, 2009, 48(2):681-686.
[8] Chien A T, Xu X, Kim J H, et al. Electrical characterization of BaTiO3 heteroepitaxial thin films by hydrothermal synthesis[J]. Journal of Materials Research, 1999, 14(8): 3330- 3339.
[9] Choi K J, Biegalski M, Li Y L, et al. Enhancement of ferroelectricity in strained BaTiO3 thin films [J]. Science, 2004, 306 (5698): 1005-1009.
[10] Christensen A N, Lundgren G, Larking I, et al. Hydrothermal Preparation of Barium Titanate by Transport Reactions [J]. Acta Chemica Scandinavica, 1970, 24(7):2447-2452.
[11] Ciftci E, Rahaman M N, Shumsky M. Hydrothermal precipitation and characterization of nanocrystalline BaTiO3 particles[J]. Journal of Materials Science, 2001, 36(20):4875-4882.
[12] Deguchi K, Nakamura E. Deviation from the Curie-Weiss Law in KH2PO4 [J]. Journal of the Physical Society of Japan, 1980, 49 (5):1887-1891.
[13] Emelyanov A Y, Pertsev N A, Hoffmann-Eifert S, et al. Grain-Boundary Effect on the Curie-Weiss Law of Ferroelectric Ceramics and Polycrystalline Thin Films: Calculation by the Method of Effective Medium[J]. Journal of Electroceramics, 2002, 9(1): 5-16.
[14] Feuersanger A E, Hagenlocher A K, Solomon A L. Preparation and Properties of Thin Barium Titanate Films [J]. Polymer Engineering & Science, 1964, 111(12): 54-59.
[15] Fousek J, Novotn á V. Manifestation of domains in the dielectric properties of ferroelectric lock-in phases [J]. Ferroelectrics, 1993, 140(1): 107-114.
[16] Glinchuk M D, Bykov I P, Kornienko S M, et al. Influence of impurities on the properties of rare-earth-doped barium-titanate ceramics [J]. Journal of Materials Chemistry, 2000, 10(4): 941-947.
[17] Gonzalo J A, Jim énez B. Ferroelectricity: The Fundamentals Collection [M]. 1951.
[18] Gottmann J, Vosseler B, Kreutz E W. Laser crystallisation during pulsed laser deposition of barium titanate thin films at low temperatures [J]. Applied Surface Science, 2002, s831-838(1):197-198.
[19] Hanske-Petitpierre O, Yacoby Y, Mustre d L J, et al. Off-center displacement of the Nb ions below and above the ferroelectric phase transition of KTa0.91Nb0.09O3 [J]. Physical Review B Condensed Matter, 1991, 44:13 (13): 6700.